Acoustic Bound States in the Continuum and Exceptional Points in Coupled Helmholtz Resonators

Mariia Krasikova,[1, 2, *] Felix Kronowetter,[2, †] Mikhail Kuzmin,[1, †] Sergey Krasikov,[1] Marcus Maeder,[2] Tao Yang,[2] Anton Melnikov,[2] Steffen Marburg,[2] and Andrey Bogdanov[1, 3, ‡]

[1]*School of Physics and Engineering, ITMO University, St. Petersburg 197101, Russia*
[2]*Chair of Vibroacoustics of Vehicles and Machines,*
Technical University of Munich, Garching b. München 85748, Germany
[3]*Harbin Engineering University, Harbin 150001, Heilongjiang , Peoples R China*
(Dated: May 14, 2024)

Resonant states underlie a variety of metastructures that exhibit remarkable capabilities for effective control of acoustic waves at subwavelength scales. The development of metamaterials relies on the rigorous mode engineering providing the implementation of the desired properties. At the same time, the application of metamaterials is still limited as their building blocks are frequently characterized by complicated geometry and can't be tuned easily. In this work, we consider a simple system of coupled Helmholtz resonators and study their properties associated with the tuning of coupling strength and symmetry breaking. We numerically and experimentally demonstrate the excitation of quasi-bound state in the continuum in the resonators placed in a free space and in a rectangular cavity. It is also shown that tuning the intrinsic losses via introducing porous inserts can lead to spectral splitting or merging of quasi-*bound states in the continuum* and occurrence of *exceptional points*. The obtained results will open new opportunities for the development of simple and easy-tunable metastructures based on Helmholtz resonances.

I. INTRODUCTION

Acoustic resonances play a pivotal role in a variety of practical applications covering all aspects of modern society, including art and entertainment [1–3], medicine [4–6], industrial applications [7, 8], and even cosmology [9]. The importance of resonances has become more prominent with the rise of metamaterials [10–12], allowing effective control over acoustic fields at the subwavelength scale. Such remarkable properties as, for instance, negative mass density [13, 14], hyperlensing [15], or subwavelength perfect absorption [16] arise from the resonant states and interplay between them. Further progress in the field of metamaterials nowadays can be associated with resonant state engineering, involving such concepts as topological states [17, 18], non-locality [19], and symmetry breaking [20].

Of particular interest in this case are the so-called *bound states in the continuum* [21, 22] (BIC), also known previously as trapped waves, which are characterized by infinitely large radiative quality factors and the associated decoupling from the far field, usually originating from the interference of several leaky modes. Firstly proposed in the field of quantum mechanics [23], BIC nowadays are actively studied in a variety of other systems, including electrical circuits [24], photonics [22, 25], and acoustics [26]. For instance, BIC can be utilized for sound confinement [27, 28], acoustic radiation enhancement [29], or improvement of noise-insulating systems [30, 31]. Since genuine BIC cannot be excited from

the far field due to the decoupling, practical applications utilize the so-called quasi-BIC, which have a large but finite radiative quality factor. The excitation of quasi-BIC is associated with the symmetry breaking allowing weak coupling with the far field [32].
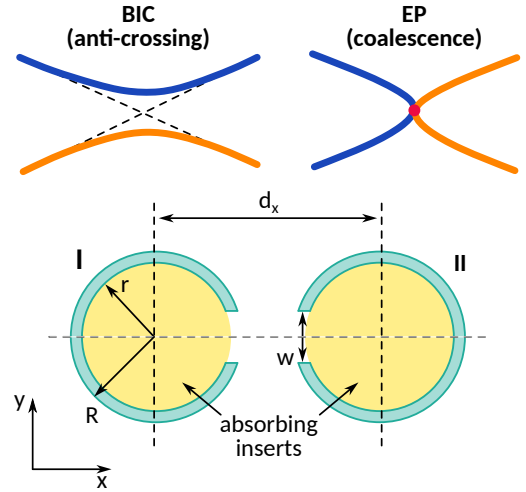

Figure 1. **Illustration of the work concept.** Bound states in the continuum (BIC) occur at the anti-crossings formed by real parts of symmetric and anti-symmetric modes in parametric space. Exceptional points (EP) represent a special case of coupling regime when the eigenmodes coalesce in the real and imaginary planes. In the considered system of two coupled Helmholtz resonators these regimes can be achieved by tuning the distance between the resonators and tuning their intrinsic losses. Both of the resonators are characterized by the inner radius r, the outer radius R and the slit width w. In addition, the volume of the resonators is supplemented by absorbing inserts.

* mariia.krasikova@metalab.ifmo.ru
† These authors contributed equally.
‡ a.bogdanov@metalab.ifmo.ru

Symmetry breaking plays a key role not only in the engineering of high-Q quasi-BICs but also in bianisotropic [33–37] and non-Hermitian systems [19, 29, 38]. In particular, *exceptional point* (EP), which denotes a condition where two or more eigenmodes and their complex eigenfrequencies coalesce, is achieved via breaking of parity (P-symmetry) and time-reversal symmetry (T-symmetry) [39–41]. EPs find today a variety of applications in photonics and acoustics [29, 42]. Practical implementations of EP in acoustic systems have enabled asymmetric field propagation [43], mode stabilization [44], and enhanced absorption [45].

Therefore, it can be inferred that such singularities as BIC and EP are pivotal for the engineering of acoustics metamaterials and devices on their base with unique functionality and performance. However, their practical implementations are still limited by the typically nontrivial geometry of unit cells and the narrow operational frequency range. Producing metastructures with easily tunable designs and acoustic properties is also a difficult task, sometimes requiring the use of non-trivial algorithms of numerical optimization. Therefore, the creation of resonant meta-atoms with straightforward designs that facilitate the easy adjustment of resonant and singular states, including BIC and EP, could greatly enhance the adoption of metamaterials in real-world applications.

In this study, we suggest and explore a straightforward design of meta-atom with easily tuned acoustic properties. The suggested meta-atom represents a pair of two-dimensional coupled C-shaped Helmholtz resonators. Such a system can be tuned via mechanical displacement of the resonators to each other as well as via the adjustment of their intrinsic losses using absorbing inserts made of conventional porous materials. We demonstrate experimentally that such a meta-atom supports quasi-BIC that could be merged into an EP via the tuning of intrinsic losses.

II. RESULTS

A. System description

The considered system consists of coupled 2D Helmholtz resonators with circular cross-sections, as shown in Fig. 1. The coupling can be tuned via the change of distance between the resonators and their mutual orientation, while the intrinsic losses can be controlled by absorbing inserts. Resonators of similar shapes were considered, for instance, in Refs. [35, 46–49]. Normal modes of such a system are formed by the superposition of the modes of solitary resonators. In-phase excitation of the resonators corresponds to a symmetric mode, which in optics is usually called a bright one since it can be directly excited and observed from the far field. On the other hand, the resonators can be excited out-of-phase, forming an anti-symmetric mode.

When an antisymmetric mode is localized entirely inside the resonators, its radiative quality factor is infinite. Such states are genuine BIC, whose coupling with the far field is prohibited by symmetry reasons. Therefore, the excitation of BIC implies a symmetry break, allowing the transformation of BIC into a quasi-BIC, whose radiative quality factor is still large but finite. Regarding eigenmodes, BIC occur in the strong mode coupling regime when the dispersion curves (real parts of eigenfrequencies) repel. For the weak coupling, the situation is reversed and the real parts of modes are crossed. In between these regimes, achieving an exceptional point (EP) in which both real and imaginary parts of the modes coalesce and the eigenmodes become linearly dependent. In the considered system, the coupling between the modes can be easily tuned via simple displacement of the resonators, affecting the radiative losses. At the same time, the intrinsic losses and coupling between the resonators can be tuned via the introduction of porous inserts into their volume. Hence, it might be expected that a simple variation of several parameters is enough to achieve the considered coupling regimes.

B. Quasi-BIC

1. Numerical Simulations

The considerations start with the resonators without absorbing inserts. For this case, the geometric parameters of the resonators were fixed to have the outer radius of the resonators $R = 30\,\mathrm{mm}$, the inner radius $r = 23\,\mathrm{mm}$, and the slit width $w = 14\,\mathrm{mm}$, which correspond to the scaled geometry considered in Refs. [48, 49]. At first, the resonators placed in a free space are considered [see Fig. 2(a)]. Such a system is characterized by two eigenmodes with symmetric and anti-symmetric field distributions [Fig. 2(b)], which correspond to the resonances of pressure spectra inside one of the resonators [Fig. 2(c)]. When the distance between the resonators becomes large enough, they almost do not interact and their eigenfrequency become almost identical corresponding to the frequency of a single Helmholtz resonator. On the contrary, the spectral width of the mode with the anti-symmetric distribution vanishes for small d_x when resonators are close to each other, which is associated with the vanishing of the imaginary parts of eigenmodes [Fig. 2(d)]. Therefore, the real parts of the modes merge with the increase of d_x, demonstrating the independent behavior of two non interacting resonators, while the imaginary parts diverge and vice versa. This is a manifestation of a symmetry-protected quasi-BIC, which becomes a genuine BIC when the imaginary part of the mode is equal to zero.
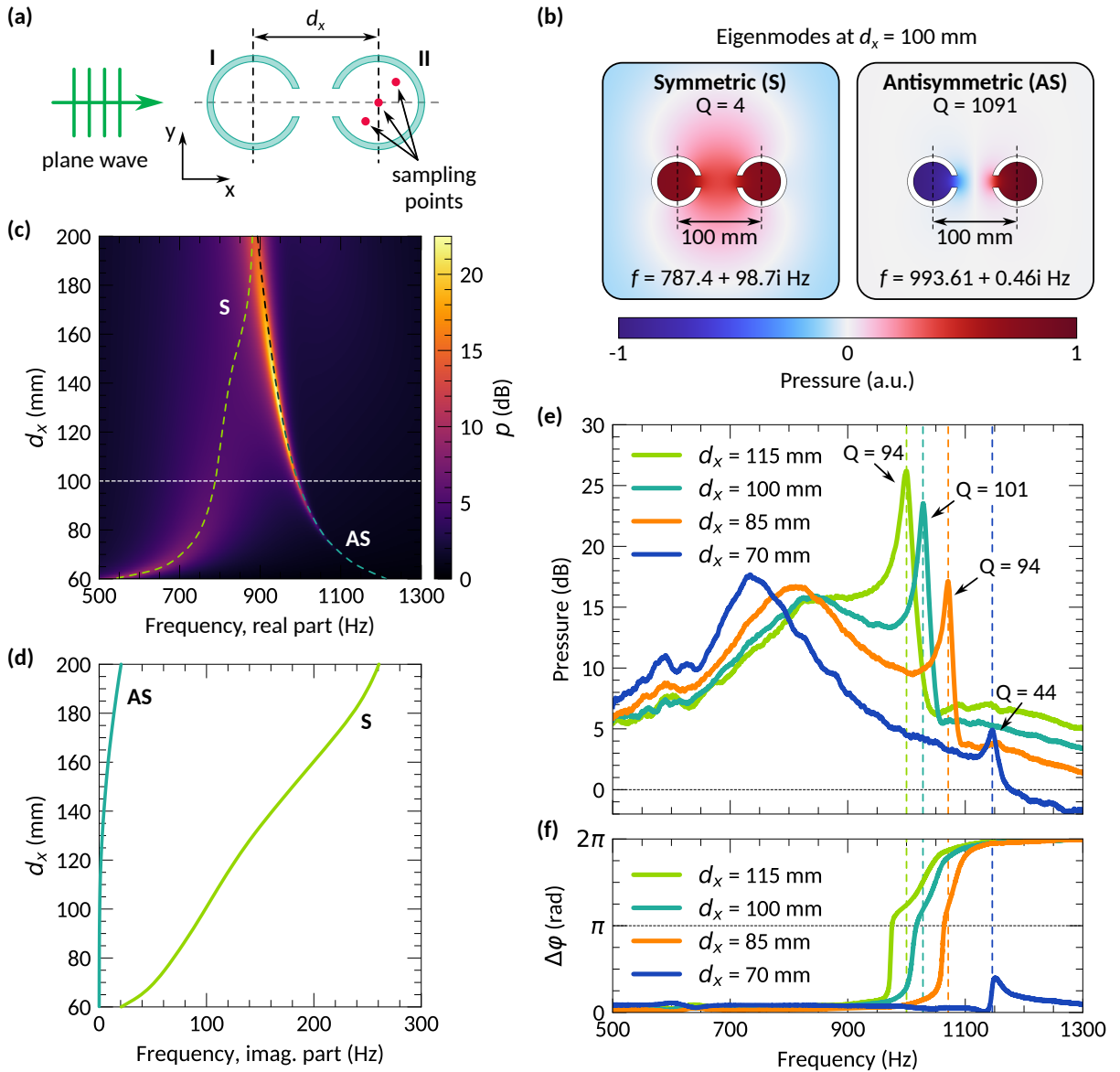
Figure 2. **Quasi-BIC in the resonators placed in a free space.** (a) Schematic illustration of the considered system. (b) Eigenmodes field distributions at $d_x = 100$ mm and their quality factor Q. (c) Pressure spectra inside one of the resonators as a function of the distance d_x between the resonators. The dashed lines indicate the corresponding eigenmodes with symmetric (S) and anti-symmetric (AS) field distributions. (d) Imaginary part of the eigenfrequencies as a function of d_x. (e) Measured pressure spectra inside one of the resonators. The values of Q indicate the corresponding quality factors of the resonances. (f) Measured spectra of phase difference between the fields inside the resonators.

2. Anechoic Chamber Measurements

The numerical calculations are verified by the measurements of pressure inside the resonators placed in the 2D anechoic chamber (see Methods). As it is shown in [Fig. 2(e)], the quasi-BIC manifests as a peak in the pressure spectra, occurring within the range $900 - -1200$ Hz, depending on the distance between the resonators. For instance, when $d_x = 100$ mm the quasi-BIC is excited at approximately 1025 Hz and its quality factor is about 100. In accordance with the numerical calculations, the

quasi-BIC shifts towards the higher frequencies with a decrease in the distance between the resonators since the coupling between the resonators becomes stronger. By definition, the anti-symmetric mode is characterized by the π phase difference between the fields inside the resonators, which can be seen from the spectra in [Fig. 2(f)], demonstrating the conventional smoothstep-like shapes. Note that for the case of $d_x = 70$ mm, the phase difference does not reach the value of π, which might be explained by the weak coupling of the antisymmetric mode with the far field. In addition, it should be noted that
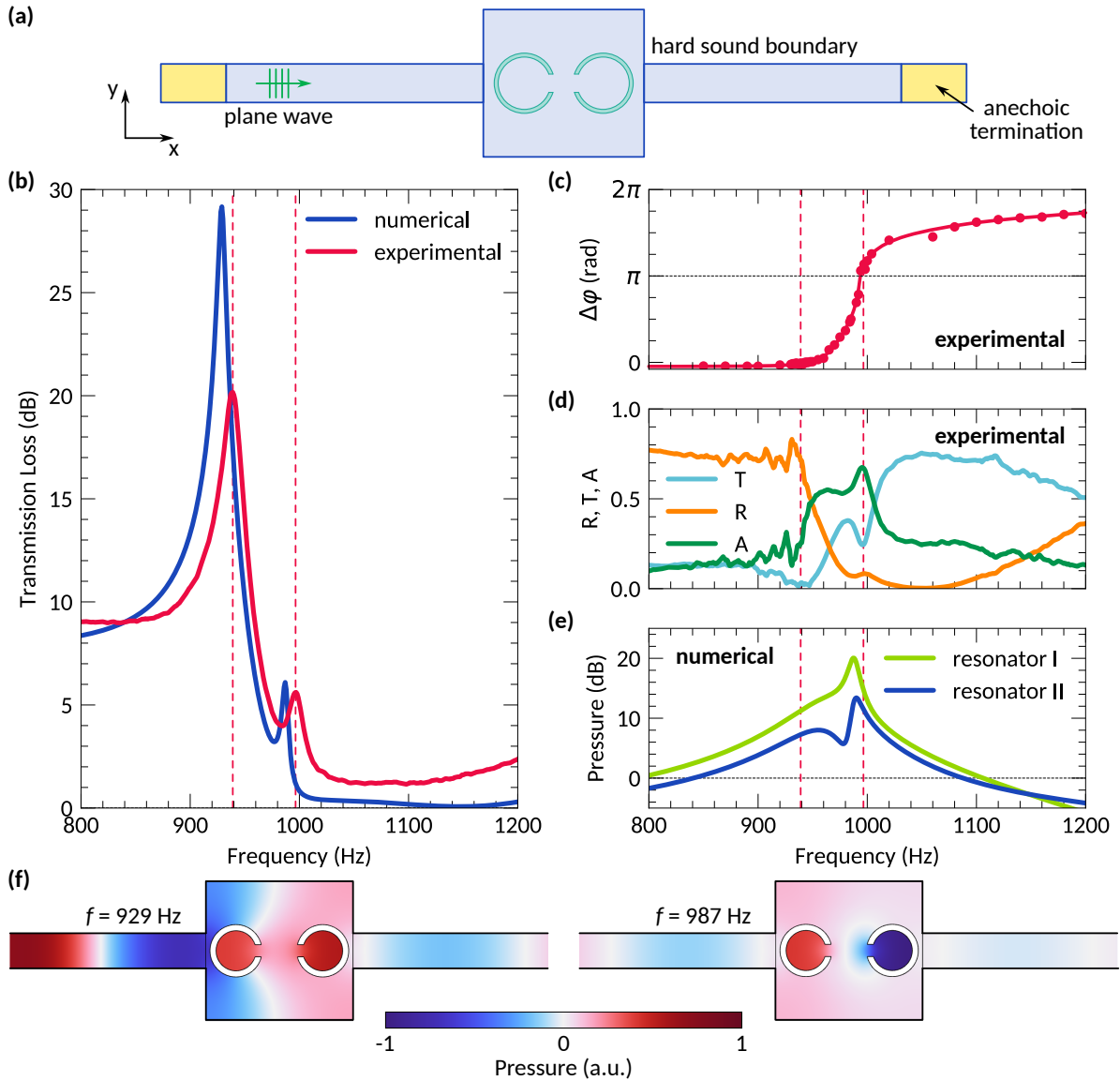
Figure 3. **Transmission tube measurements of quasi-BIC.** (a) Schematic illustration of the system consisting of the box with the resonators embedded into the transmission tube. (b) Transmission loss spectra. (c) Measured spectra of phase difference between the fields inside the resonators. (d) Experimentally obtained reflection, transmission and absorption coefficients. (e) Pressure spectra calculated inside the resonators. (f) Field distributions corresponding to the transmission loss resonances occurring near 929 Hz and 987 Hz.

the resonances of the measured spectra are shifted from the numerically calculated ones by approximately 30 Hz–50 Hz, which arises from manufacturing errors as sub-millimeter changes in the resonators sizes affect the position of the resonances (see Supplementary Information). However, the experimental results are in good agreement with those from numerical simulations, cf. Figs. 2(c) and 2(e) as well as the Supplementary Information.

3. Transmission Tube Measurements

While the quasi-BIC mode is weakly coupled to the far field, it is also almost decoupled from the other modes of the system. Hence, it can be expected that the quasi-BIC can still be excited even if the environment of the resonators changes. For instance, the resonators can be placed inside a rectangular cavity [see Fig. 3(a)], which actually by itself supports quasi-BIC [50]. When the anti-symmetric modes of the cavity and the resonators do not interact, the transmission loss spectra of such a system should also demonstrate a high-Q peak near the frequency corresponding to the quasi-BIC occurring for the
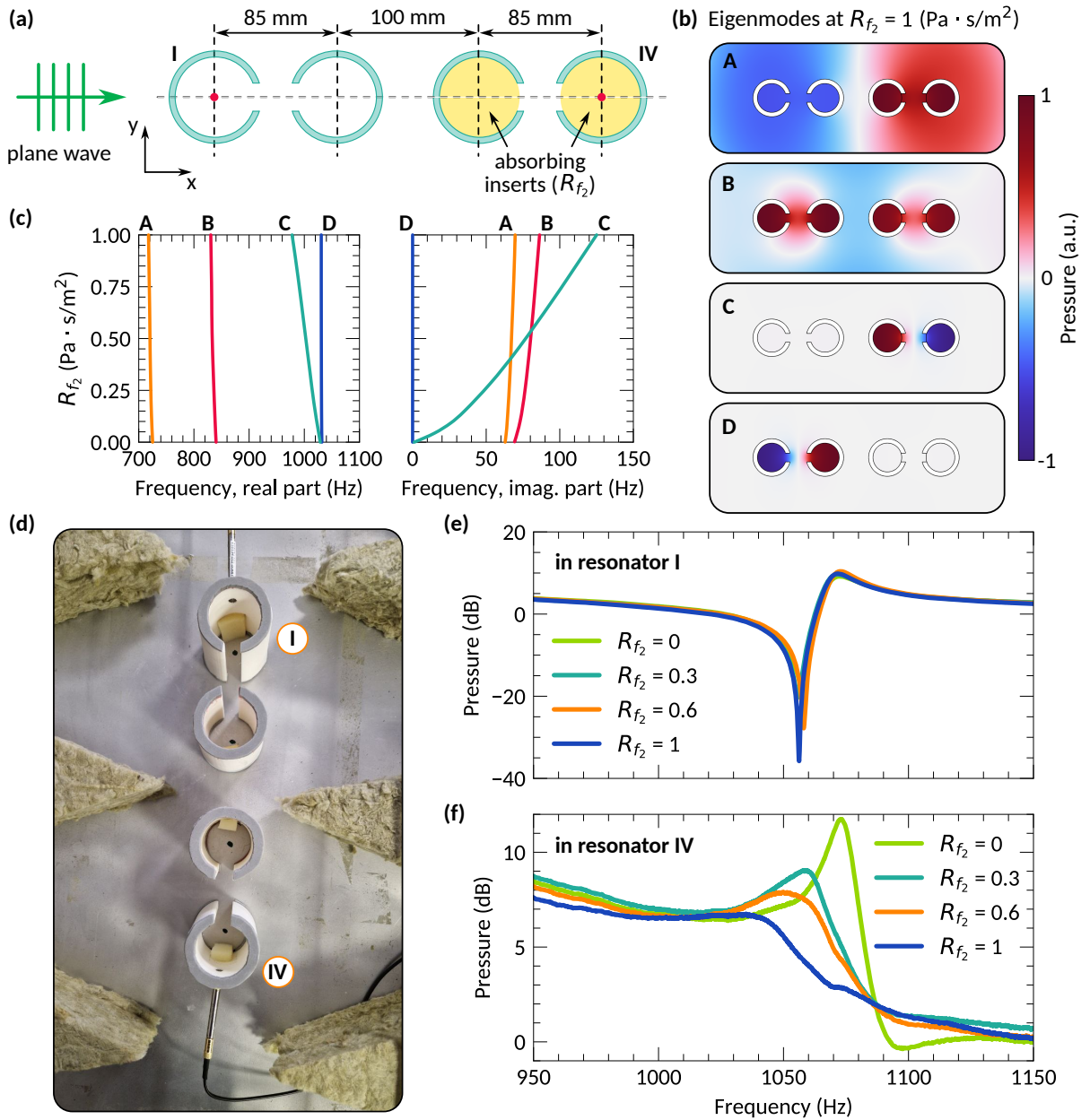
Figure 4. **Splitting of quasi-BIC** (a) Schematic illustration of the considered system consisting of two pairs of coupled resonators placed in a free space. One of the pairs is supplemented by porous inserts with the flow resistivity R_{f_2}. (b) Eigenmodes field distributions for the case of $R_{f_2} = 1\,\mathrm{Pa \cdot s/m^2}$ and (c) real and imaginary parts of eigenmodes for different values of R_{f_2}. (d) Photo of the samples. Experimentally obtained pressure spectra measured inside (e) the resonator I and (f) the resonator IV.

case of the resonators in a free space. Indeed, Fig. 3(b) shows the presence of the two pronounced peaks near 940 Hz and 1000 Hz, obtained via the impedance tube measurements (see Methods). These peaks expected correspond to the peaks of the pressure spectra calculated inside the resonators [see Fig. 3(e)]. Again, the phase difference between the fields inside the resonators represents the smooth step-like curve [see Fig. 3(c)], demonstrating that the phase difference is nearly $\Delta\varphi = \pi$ at the quasi-BIC frequency. The peak of the transmission

loss spectrum occurring near 940 Hz can be associated with the symmetric excitation of Helmholtz resonators [see Fig. 3(f)], leading to the decrease of the transmission coefficient [Fig. 3(d)]. At the same time, the second peak in the transmission spectra, occurring near 1000 Hz, corresponds to the quasi-BIC characterized by the antisymmetric field distribution, as previously [see Fig. 3(f)]. The resonance in the transmission loss, in this case, is related to the increase of the absorption coefficient [see Fig. 3(d)]. However, it should be noted that the trans-

mission loss in the considered case is probably associated with energy leakage into the mechanical vibrations of the box walls, which are not taken into account in the numerical calculations.

C. Tuning of Intrinsic Losses

Apart from the distance between the resonators, the resonances can be controlled by introducing porous materials into the volume of the resonators. Such inserts may significantly decrease the quality factor of a standalone Helmholtz resonator (see Supplementary Information), practically leading to the destruction of the resonance. However, small intrinsic losses can be used for the fine-tuning of quasi-BIC. For instance, the system supplemented by an additional pair of the resonators can be considered, such that this additional pair is supplemented by the absorbing inserts made of a porous material with the flow resistivity R_{f_2}, while another pair has no such inserts [see Fig. 4(a)]. Since there are four resonators in such a system, it is characterized by four eigenmodes [see Figs. 4(b)], two of which are characterized by the symmetric field distributions within the pairs and two – by the antisymmetric [see Figs. 4(c)]. When the flow resistivity R_{f_2} is zero, the antisymmetric eigenmodes are nearly degenerate, meaning that the have equal real parts of the frequencies, but slightly different values for the imaginary parts. Both the real and imaginary parts of the symmetric modes are almost not affected by the change of R_{f_2}. At the same time, the increase of R_{f_2} results in the splitting of quasi-BIC [see Figs. 4(b) and 4(c)], such that the frequency of one antisymmetric eigenmode remains the same, while another antisymmetric eigenmode shifts towards the smaller real frequencies, while its quality factor quickly decreases. Similar behaviour can be also observed experimentally. In this case the spectral position of the quasi-BIC measured in the first pair remains nearly unchanged [see Fig. 4(e)], while the quasi-BIC measured in the second pair shifts towards the lower frequencies with the increase of the absorbing insert size [see Fig. 4(d)]. These results indicate the spectral positions of BIC in arrays of Helmholtz resonators can be fine-tuned via simple adjustment of the intrinsic losses controlled by the size of the absorbing inserts.

The important remark is that in the numerical calculations, the insert occupies the whole volume of the resonator, and the corresponding porous material is characterized only by the flow resistivity, which is varied. For the experimental verification, it is assumed that a small piece of porous material with a large flow resistivity is roughly equivalent to a large piece of a material with a low flow resistivity. In such an approximation, a porous insert occupying the whole volume of the resonator can be represented by an insert occupying only a part of the volume [see Fig. 4(d)], and it is much easier to control the size of an insert contrary to its material parameters.

To push the concept further, the considered system of two pairs of coupled resonators can be used to achieve an EP. For that, both pairs of the resonators should be supplemented by porous inserts, such that in the first pair, the inserts are characterized by the flow resistivity R_{f_1} and in the second pair – by R_{f_2} [see Fig. 5(a)]. The tuning of the flow resistivity allows to control both antisymmetric eigenmodes and achieve their coalescence. As shown in Figs. 5(b) and 5(d), when $R_{f_1} = 1\,\mathrm{Pa \cdot s/m^2}$ and $R_{f_2} \approx 0.5\,\mathrm{Pa \cdot s/m^2}$ these eigenmodes have the same complex frequency, which can be considered as the manifestation of an EP. To verify this result experimentally, the pressure spectra is measured inside the first and the last resonator using the porous inserts of different size, similarly to the idea developed in Ref. [51]. The merging of the antisymmetric eigenmodes in this case should occur as the spectral overlap of the quasi-BIC measured in both pairs. To provide such measurements, the size of the porous inserts inside the first pair is fixed, while the size of the inserts in the second pair is varied. Hence, the quasi-BIC occurring in the first pair remains almost unchanged [see Fig. 5(c)], while the spectral position of the quasi-BIC in the second pair shifts, such that when R_{f_2} is smaller than R_{f_1}, the quasi-BIC in both pairs are excited at the same frequency [see Fig. 5(e)]. While the exact values of the flow resistivity are not estimated in this work, it still can be concluded that the provided measurements indirectly confirm the presence of the EP in the considered system.

III. CONCLUSION

In this work, coupling regimes of 2D Helmholtz resonators were investigated. It was shown that quasi-BIC and EP can be easily achieved by tuning the geometric parameters and intrinsic losses of the resonators. Experimental demonstrations reveal the resonant enhancement of absorption associated with quasi-BIC.The obtained results aim to extend the possibilities of physics-based design of metamaterials and pave the route towards novel devices for the efficient control of acoustic fields at the subwavelength scales.

IV. METHODS

A. Experimental measurements

For the resonators placed in a free space, the measurements are performed in the 2D anechoic chamber, representing a waveguide with walls covered by absorbing mineral wool [see Figs. 6(a) and 6(b)]. In particular, the walls and the bottom of the waveguide are made of 15 mm thick aluminum plates, and the lid is made of 6 mm plexiglass. Since the impedance contrast between air and most of the solid materials is huge [52], the lid and the bottom can be considered as sound hard walls.
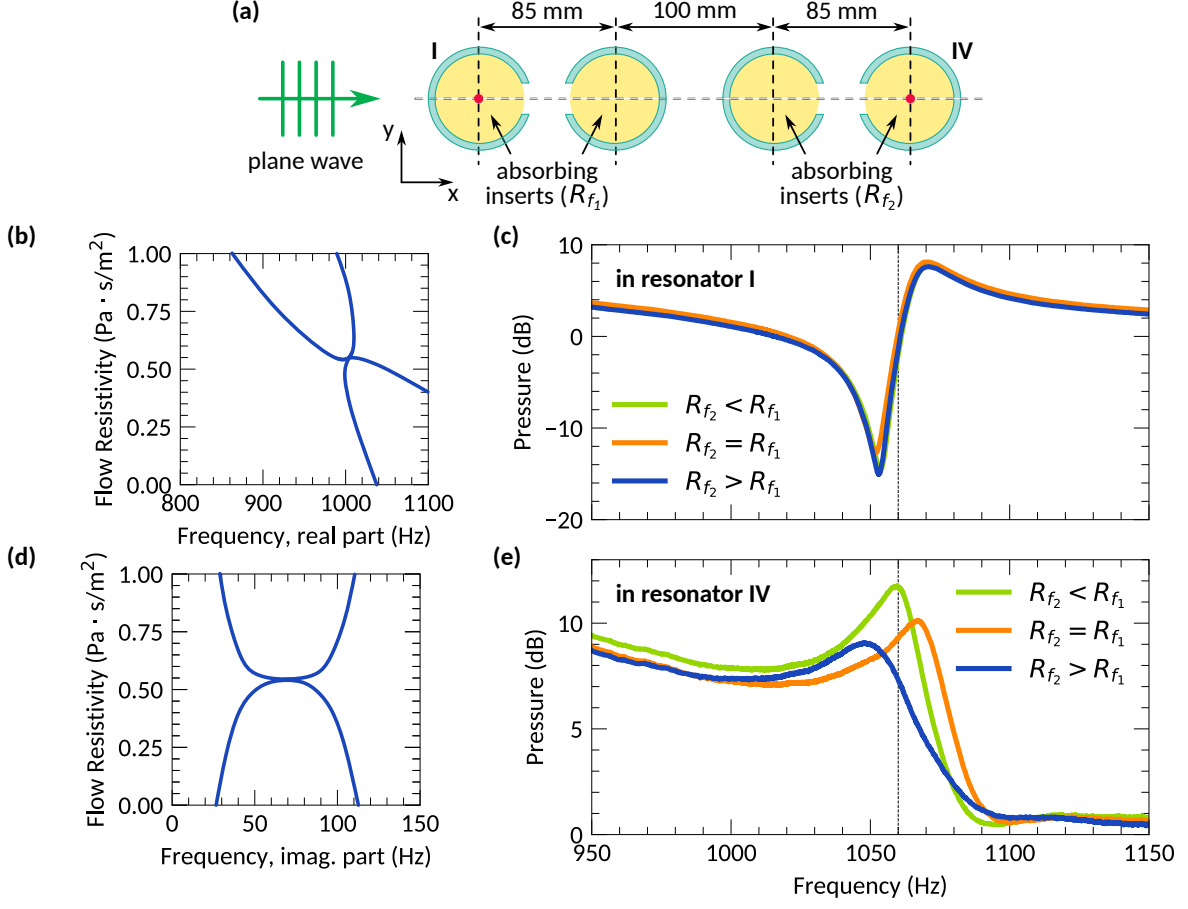
Figure 5. **EP in the system of four resonators.** (a) Schematic illustration of the considered system consisting of two pairs of coupled resonators, both supplemented by porous inserts with the flow resistivity R_{f_1} and R_{f_2}, respectively. (b) The real and (d) imaginary parts of eigenmodes for the different values of R_{f_2}. Experimentally obtained pressure spectra measured inside (c) the resonator I and (e) the resonator IV. The results shwon in panels (b)–(e) are obtained for $R_{f_1} = 1\,\mathrm{Pa} \cdot \mathrm{s/m}^2$.

The height of the waveguide is 60 mm, while the width and the length are 650 mm and 1350 mm, respectively. The thickness of the mineral wood inserts is 300 mm (from a wall to the tip of a pyramid). Generation and recording of the sound signal is done using the analysis system Crysound CRY6151B and 1/4" pressure field microphone Crysound CRY342. The resonators themselves are fabricated by additive manufacturing technology on the Bambu Lab X1-Carbon 3D printer (Shenzhen Tuozhu Technology Co., Ltd., Shenzhen, China). To avoid gaps between the resonators and the lids, the top of the resonators are supplemented by thin porous inserts.

The transmission loss measurements are conducted in the AED AcoustiTube measurement system, the impedance tube. In this case, the resonators are placed in a box with a rectangular cross-section [see Fig. 6(c) and 6(d)]. The width of the box is 170 mm, the height is 160 mm, and the thickness is 40 mm. The scattering coefficients are extracted from the measured T-matrix

coefficients using the conventional expressions [53] as:

$$t^- = \frac{2e^{ikL}}{T_{11} + T_{12}/Z_L + T_{21}Z_0 + T_2 2Z_0/Z_L}, \quad (1)$$

$$t^+ = \frac{Z_0}{Z_L} \frac{2e^{ikL}(T_{11}T_{22} - T_{12}T_{21})}{T_{11} + T_{12}/Z_L + T_{21}Z_0 + T_2 2Z_0/Z_L}, \quad (2)$$

$$r^- = \frac{T_{11} + T_{12}/Z_L - T_{21}Z_0 - T_2 2Z_0/Z_L}{T_{11} + T_{12}/Z_L + T_{21}Z_0 + T_2 2Z_0/Z_L}, \quad (3)$$

$$r^+ = \frac{-T_{11} + T_{12}/Z_L - T_{21}Z_0 + T_2 2Z_0/Z_L}{T_{11} + T_{12}/Z_L + T_{21}Z_0 + T_2 2Z_0/Z_L}, \quad (4)$$

where Z_0, Z_L are acoustic impedances of the media at the sides of the structure, such that L is the thickness of the structure, and the superscripts indicate the positive $(+)$ and $(-)$ negative direction of the incident wave propagation. The amplitude coefficients then can be defined as $T^{+,-} = |t^{+,-}|^2$ and $R^{+,-} = |r^{+,-}|^2$. Correspondingly, the absorption coefficients can be defined as $A^{+,-} = 1 - |r^{+,-}|^2 - |t^{+,-}|^2$. When the system is symmetric, $A = A^+ = A^-$. Note that all measured spectra
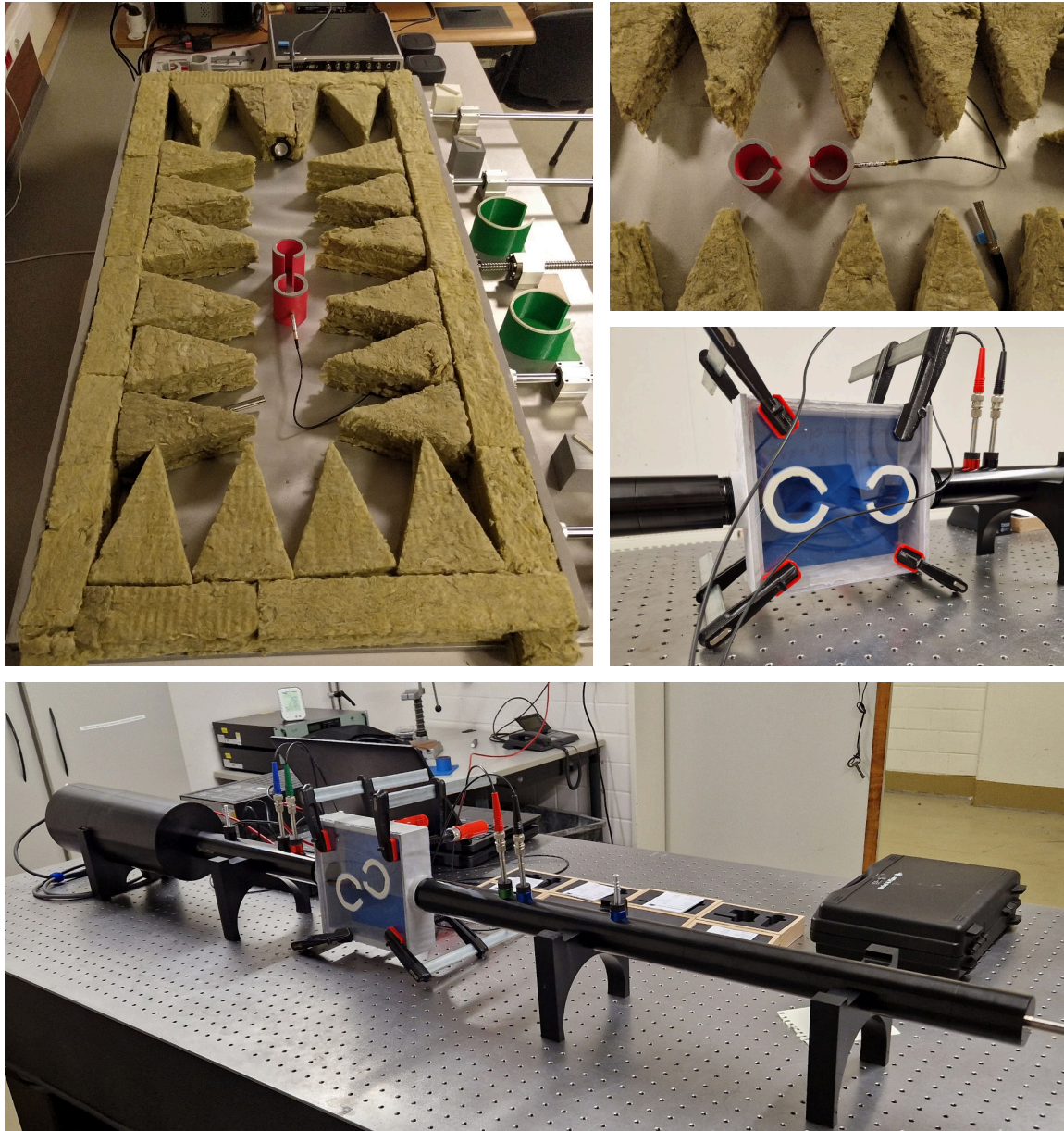
Figure 6. **Experimental Setups.** (a) Photo of the 2D anechoic chamber imitating a free space. Close up photo of (b) the samples used in the 2D anechoic chamber and (c) the samples and the box used for the transmission tube measurements. (d) Photo of the transmission tube setup.

are slightly smoothed using the Savitzky-Golay filter of order 3 and with a window width of 11.

B. Numerical calculations

All numerical calculations are performed in COMSOL Multiphysics using the "Pressure Acoustics" physics. The incident plane wave is introduced as the background pressure field with the amplitude $p_0 = 1\,\mathrm{Pa}$. The pressure inside the resonators is defined as a root mean square of pressure calculated at several sampling points located inside the resonators. In order to account for the thermoviscous dissipation in the boundary layer of the resonators' walls, the "Thermoviscous Boundary Layer Impedance" condition is applied to the corresponding boundaries. Porous inserts are included via the "Poroacoustics" feature utilizing the Delany-Bazley-Miki model.

BASIS foundation.

V. AUTHOR CONTRIBUTIONS

M.Kr., M.K., F.K., M.M., and T.Y. performed the experimental measurements, M.Kr., S.K. and F.K. provided numerical calculations. S.K. and M.Kr. suggested the idea and developed the concept of the work. A.M., M.M., S.M. and A.B. supervised the project. All authors contributed to writing and editing of the manuscript.

VI. COMPETING INTERESTS

The authors declare no competing interests.

[1] Michael E. McIntyre, Robert T. Schumacher Schumacher, and Jim Woodhouse. On the oscillations of musical instruments. *The Journal of the Acoustical Society of America*, 74(5):1325–1345, November 1983.

[2] Robert G. Arns and Bret E. Crawford. Resonant Cavities in the History of Architectural Acoustics. *Technology and Culture*, 36(1):104–135, 1995.

[3] Joe Wolfe, Maëva Garnier, and John Smith. Vocal tract resonances in speech, singing, and playing musical instruments. *HFSP Journal*, 3(1):6–23, February 2009.

[4] Ross M. Henderson. Essential physics of nuclear acoustic resonance imaging. In *Medical Imaging 1997: Physics of Medical Imaging*, volume 3032, pages 142–152. SPIE, May 1997.

[5] Lennart D. Johns. Nonthermal Effects of Therapeutic Ultrasound: The Frequency Resonance Hypothesis. *Journal of Athletic Training*, 37(3):293–299, 2002.

[6] Kerstin Länge, Bastian E. Rapp, and Michael Rapp. Surface acoustic wave biosensors: A review. *Analytical and Bioanalytical Chemistry*, 391(5):1509–1519, July 2008.

[7] Robert G. Leisure and Frank A. Willis. Resonant ultrasound spectroscopy. *Journal of Physics: Condensed Matter*, 9(28):6001, July 1997.

[8] Ming Yuan, Ziping Cao, Jun Luo, and Xiujian Chou. Recent Developments of Acoustic Energy Harvesting: A Review. *Micromachines*, 10(1):48, January 2019.

[9] C. Aerts. Probing the interior physics of stars through asteroseismology. *Reviews of Modern Physics*, 93(1):015001, January 2021.

[10] Steven A. Cummer, Johan Christensen, and Andrea Alù. Controlling sound with acoustic metamaterials. *Nature Reviews Materials*, 1(3):1–13, February 2016.

[11] Guancong Ma and Ping Sheng. Acoustic metamaterials: From local resonances to broad horizons. *Science Advances*, 2(2):e1501595, February 2016.

[12] Badreddine Assouar, Bin Liang, Ying Wu, Yong Li, Jian-Chun Cheng, and Yun Jing. Acoustic metasurfaces. *Nature Reviews Materials*, 3(12):460–472, December 2018.

[13] Sam Hyeon Lee, Choon Mahn Park, Yong Mun Seo, Zhi Guo Wang, and Chul Koo Kim. Acoustic metamaterial with negative density. *Physics Letters A*, 373(48):4464–4469, December 2009.

[14] Jensen Li and C. T. Chan. Double-negative acoustic metamaterial. *Physical Review E*, 70(5):055602, November 2004.

[15] Jensen Li, Lee Fok, Xiaobo Yin, Guy Bartal, and Xiang Zhang. Experimental demonstration of an acoustic magnifying hyperlens. *Nature Materials*, 8(12):931–934, December 2009.

[16] Yong Li and Badreddine M. Assouar. Acoustic metasurface-based perfect absorber with deep subwavelength thickness. *Applied Physics Letters*, 108(6):063502, February 2016.

[17] Haoran Xue, Yihao Yang, and Baile Zhang. Topological acoustics. *Nature Reviews Materials*, 7(12):974–990, December 2022.

[18] Xiujuan Zhang, Farzad Zangeneh-Nejad, Ze-Guo Chen, Ming-Hui Lu, and Johan Christensen. A second wave of topological phenomena in photonics and acoustics. *Nature*, 618(7966):687–697, June 2023.

[19] Xu Wang, Ruizhi Dong, Yong Li, and Yun Jing. Nonlocal and non-Hermitian acoustic metasurfaces. *Reports on Progress in Physics*, 86(11):116501, October 2023.

[20] Hussein Nassar, Behrooz Yousefzadeh, Romain Fleury, Massimo Ruzzene, Andrea Alù, Chiara Daraio, Andrew N. Norris, Guoliang Huang, and Michael R. Haberman. Nonreciprocity in acoustic and elastic materials. *Nature Reviews Materials*, 5(9):667–685, September 2020.

[21] Chia Wei Hsu, Bo Zhen, A. Douglas Stone, John D. Joannopoulos, and Marin Soljačić. Bound states in the continuum. *Nature Reviews Materials*, 1(9):1–13, July 2016.

[22] Kirill L. Koshelev, Zarina F. Sadrieva, Alexey A. Shcherbakov, Yu.S. Kivshar, and Andrey A. Bogdanov. Bound states in the continuum in photonic structures. *Physics-Uspekhi*, 66(05):494–517, May 2023.

[23] John von Neumann and Eugene. P. Wigner. Über merkwürdige diskrete Eigenwerte. In Arthur S. Wightman, editor, *The Collected Works of Eugene Paul Wigner: Part A: The Scientific Papers*, The Collected Works of Eugene Paul Wigner, pages 291–293. Springer, Berlin, Heidelberg, 1993.

[24] Zhuangzhuang Li, Jien Wu, Xueqin Huang, Jiuyang Lu, Feng Li, Weiyin Deng, and Zhengyou Liu. Bound state in the continuum in topological inductor–capacitor circuit. *Applied Physics Letters*, 116(26):263501, June 2020.

[25] Meng Kang, Tao Liu, C. T. Chan, and Meng Xiao. Applications of bound states in the continuum in photonics. *Nature Reviews Physics*, 5(11):659–678, November 2023.

[26] Almas F. Sadreev. Interference traps waves in an open system: Bound states in the continuum. *Reports on Progress in Physics*, 84(5):055901, April 2021.

[27] Sibo Huang, Tuo Liu, Zhiling Zhou, Xu Wang, Jie Zhu, and Yong Li. Extreme Sound Confinement From Quasibound States in the Continuum. *Physical Review Applied*, 14(2):021001, August 2020.

[28] Ilya Deriy, Ivan Toftul, Mihail Petrov, and Andrey Bogdanov. Bound States in the Continuum in Compact Acoustic Resonators. *Physical Review Letters*, 128(8):084301, February 2022.

[29] Sibo Huang, Shuhuan Xie, He Gao, Tong Hao, Shuang Zhang, Tuo Liu, Yong Li, and Jie Zhu. Acoustic Purcell effect induced by quasibound state in the continuum. *Fundamental Research*, 4(1):57–62, January 2024.

[30] Liyun Cao, Yifan Zhu, Sheng Wan, Yi Zeng, Yong Li, and Badreddine Assouar. Perfect absorption of flexural waves induced by bound state in the continuum. *Extreme Mechanics Letters*, 47:101364, August 2021.

[31] Haiyan Zhang, Shanshan Liu, Zhiwei Guo, Shengyu Hu, Yuguang Chen, Yunhui Li, Yong Li, and Hong Chen. Topological bound state in the continuum induced unidirectional acoustic perfect absorption. *Science China Physics, Mechanics & Astronomy*, 66(8):284311, July 2023.

[32] Kirill Koshelev, Sergey Lepeshov, Mingkai Liu, Andrey Bogdanov, and Yuri Kivshar. Asymmetric Metasurfaces with High-Q Resonances Governed by Bound States in the Continuum. *Physical Review Letters*, 121(19):193903, November 2018.

[33] Viktar S. Asadchy, Ana Díaz-Rubio, and Sergei A. Tretyakov. Bianisotropic metasurfaces: Physics and applications. *Nanophotonics*, 7(6):1069–1094, June 2018.

[34] Steven R. Craig, Xiaoshi Su, Andrew Norris, and Chengzhi Shi. Experimental Realization of Acoustic Bianisotropic Gratings. *Physical Review Applied*, 11(6):061002, June 2019.

[35] Anton Melnikov, Yan Kei Chiang, Li Quan, Sebastian Oberst, Andrea Alù, Steffen Marburg, and David Powell. Acoustic meta-atom with experimentally verified maximum Willis coupling. *Nature Communications*, 10(1):3148, 2019.

[36] Junfei Li, Ailing Song, and Steven A. Cummer. Bianisotropic Acoustic Metasurface for Surface-Wave-Enhanced Wavefront Transformation. *Physical Review Applied*, 14(4):044012, October 2020.

[37] Anton Melnikov, Sören Köble, Severin Schweiger, Yan Kei Chiang, Steffen Marburg, and David A. Powell. Microacoustic Metagratings at Ultra-High Frequencies Fabricated by Two-Photon Lithography. *Advanced Science*, 9(20):2200990, 2022.

[38] Yuto Ashida, Zongping Gong, and Masahito Ueda. Non-Hermitian physics. *Advances in Physics*, 69(3):249–435, July 2020.

[39] Walter D. Heiss. The physics of exceptional points. *Journal of Physics A: Mathematical and Theoretical*, 45(44):444016, October 2012.

[40] Ş K. Özdemir, S. Rotter, F. Nori, and L. Yang. Parity–time symmetry and exceptional points in photonics. *Nature Materials*, 18(8):783–798, August 2019.

[41] Vladimir Igoshin, Mariia Tsimokha, Anastasia Nikitina, Mihail Petrov, Ivan Toftul, and Kristina Frizyuk. Exceptional points in single open acoustic resonator due to symmetry breaking. *Physical Review B*, 109(14):144102, April 2024.

[42] Mohammad-Ali Miri and Andrea Alù. Exceptional points in optics and photonics. *Science*, 363(6422):eaar7709, January 2019.

[43] Chen Shen, Junfei Li, Xiuyuan Peng, and Steven A. Cummer. Synthetic exceptional points and unidirectional zero reflection in non-Hermitian acoustic systems. *Physical Review Materials*, 2(12):125203, December 2018.

[44] Claire Bourquard and Nicolas Noiray. Stabilization of acoustic modes using Helmholtz and Quarter-Wave resonators tuned at exceptional points. *Journal of Sound and Vibration*, 445:288–307, April 2019.

[45] Vassos Achilleos, Georgios Theocharis, Olivier Richoux, and Vincent Pagneux. Non-Hermitian acoustic metamaterials: Role of exceptional points in sound absorption. *Physical Review B*, 95(14):144303, April 2017.

[46] Anton Melnikov, Marcus Maeder, Niklas Friedrich, Yan Pozhanka, Alexander Wollmann, Michael Scheffler, Sebastian Oberst, David Powell, and Steffen Marburg. Acoustic metamaterial capsule for reduction of stage machinery noise. *The Journal of the Acoustical Society of America*, 147(3):1491–1503, March 2020.

[47] Felix Kronowetter, Lisa Pretsch, Yan Kei Chiang, Anton Melnikov, Shahrokh Sepehrirahnama, Sebastian Oberst, David A. Powell, and Steffen Marburg. Sound attenuation enhancement of acoustic meta-atoms via coupling. *The Journal of the Acoustical Society of America*, 154(2):842–851, August 2023.

[48] Mariia Krasikova, Sergey Krasikov, Anton Melnikov, Yuri Baloshin, Steffen Marburg, David A. Powell, and Andrey Bogdanov. Metahouse: Noise-Insulating Chamber Based on Periodic Structures. *Advanced Materials Technologies*, 8(1):2200711, 2023.

[49] Mariia Krasikova, Aleksandra Pavliuk, Sergey Krasikov, Mikhail Kuzmin, Andrey Lutovinov, Anton Melnikov, Yuri Baloshin, David A. Powell, Steffen Marburg, and Andrey Bogdanov. Broadband noise-insulating periodic structures made of coupled Helmholtz resonators. *APL Materials*, 12(1), January 2024.

[50] Felix Kronowetter, Marcus Maeder, Yan Kei Chiang, Lujun Huang, Johannes D. Schmid, Sebastian Oberst, David A. Powell, and Steffen Marburg. Realistic prediction and engineering of high-Q modes to implement stable Fano resonances in acoustic devices. *Nature Communications*, 14(1):6847, October 2023.

[51] Kun Ding, Guancong Ma, Meng Xiao, Z. Q. Zhang, and C. T. Chan. Emergence, Coalescence, and Topological Properties of Multiple Exceptional Points and Their Experimental Realization. *Physical Review X*, 6(2):021007, April 2016.

[52] Alan R. Selfridge. Approximate Material Properties in Isotropic Materials. *IEEE Transactions on Sonics and Ultrasonics*, 32(3):381–394, May 1985.

[53] Noé Jiménez, Olga Umnova, and Jean-Philippe Groby, editors. *Acoustic Waves in Periodic Structures, Metamaterials, and Porous Media: From Fundamentals to Industrial Applications*, volume 143 of *Topics in Applied Physics*. Springer International Publishing, Cham, 2021.

Supplementary Information for
Acoustic Bound States in the Continuum and Exceptional Points in Coupled Helmholtz Resonators

S1. COMPARISON OF THE EXPERIMENTAL AND NUMERICAL RESULTS

The experimental results presented in the main text are in a good agreement with the numerical calculations. However, the resonant peaks in the pressure and transmission loss spectra are noticeably shifted with respect to each other. Such a difference can be explained by the limited accuracy of the samples manufacturing. For instance, even slight inaccuracies of order $0.5\,\mathrm{mm}$ may lead to the significant shift of the transmission loss resonances, as shown in Fig. S1. The corresponding measured spectrum lies within the range of the numerical curves, and hence it can be concluded that the experimental results reproduce the numerical ones.
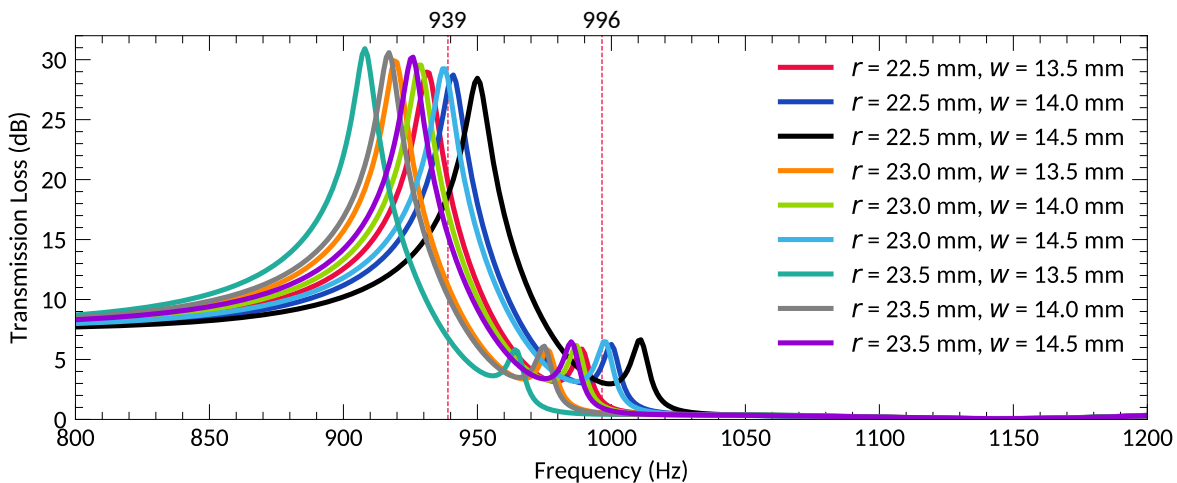

Figure S1. **The influence of the geometric parameters of the resonators on numerical calculations**. Transmission loss spectra for the case of two coupled resonators place in the rectangular box. The distance between the resonators is $d_x = 100\,\mathrm{mm}$ and the outer radius is $R = 30\,\mathrm{mm}$, while the inner radius r and the slit width w are varied. The vertical dashed lines indicate the position of peaks in the experimentally measured spectra.

It is also should be mentioned that when a pair of the resonators is considered the pressure spectra inside them are slightly different. In particular, the pressure spectra measured and calculated inside one of the resonators are characterized by Fano-shaped resonances corresponding to the antisymmetric mode [see Figs. S2(b) and S2(d)], while for the second resonator the corresponding peaks have Lorentzian-like shape [see Figs. S2(c) and S2(e)].
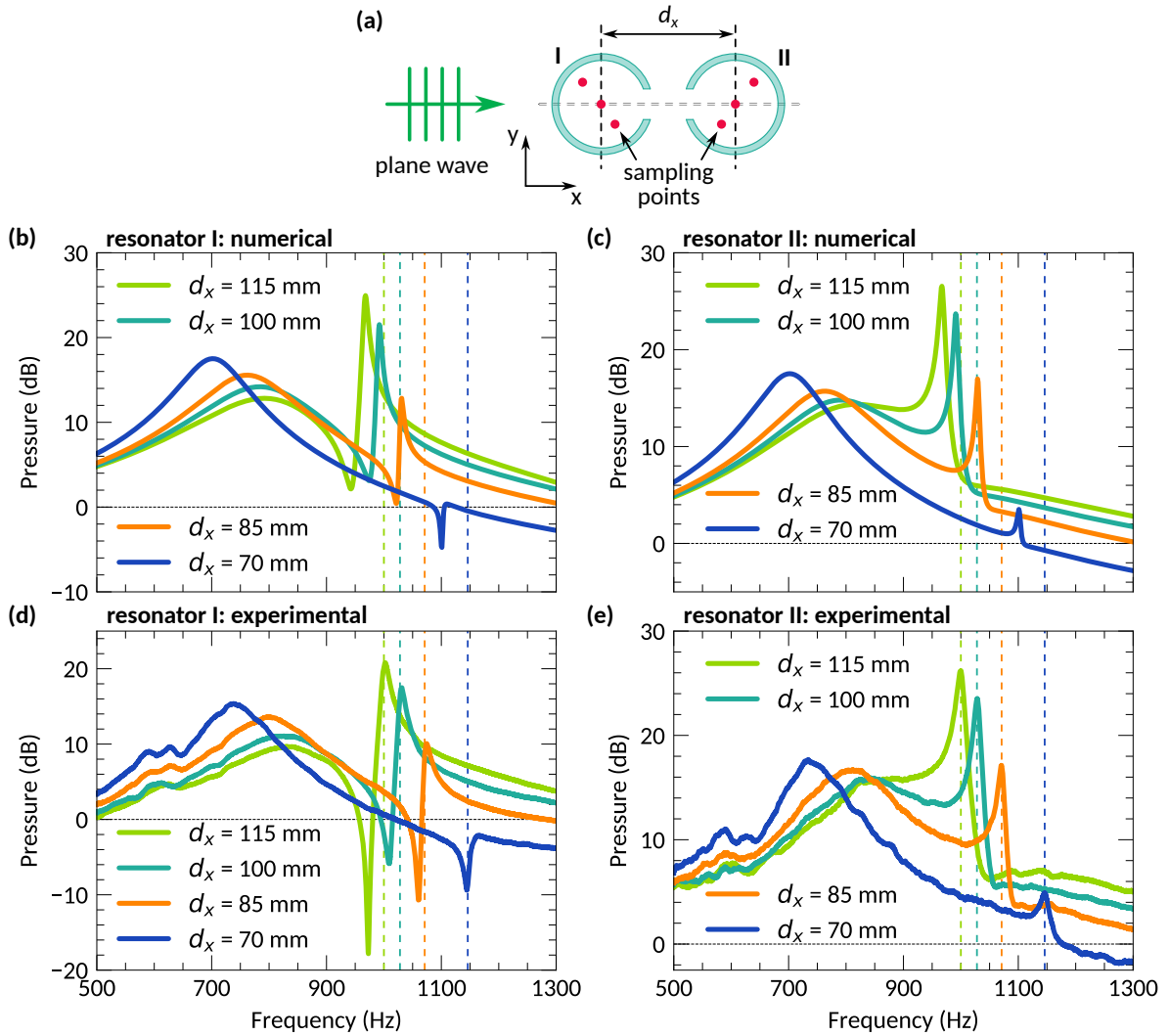
Figure S2. **Pressure spectra in the open system of coupled resonators.** (a) Schematic illustration of the system consisting of two resonators excited by a plane wave. The pressure spectra (b) calculated and (d) measured inside the resonator I and the corresponding spectra (c) calculated and (e) measured inside the resonator II.

S2.   TUNING OF INTRINSIC LOSSES

While the main text is dedicated to the systems of coupled resonators, it is still reasonable to analyse a standalone resonator. In particular, two configurations are considered, such that the resonator is oriented "away" from and "towards" the incident field [see Fig. S3(a) and S3(b)]. In both cases the resonance occurs near 900 Hz, though for the configuration A the pressure is slightly than for the B [see Fig. S3(c)]. When the resonator is supplemented by a porous insert, the spectral width of the resonance increases with the increase of the flow resistivity, while the pressure decreases [see Fig. S3(d) – S3(f)]. Large values of the flow resistivity practically result in the disappearance

of the resonance as the intrinsic losses become too large and the pressure spectra flattens. Hence, even for the case of a standalone resonator it is reasonable to consider small values of flow resistivity, which can be achieved via considerations of the partial inserts, occupying only a small part of the resonator's volume, as discussed in the main text.
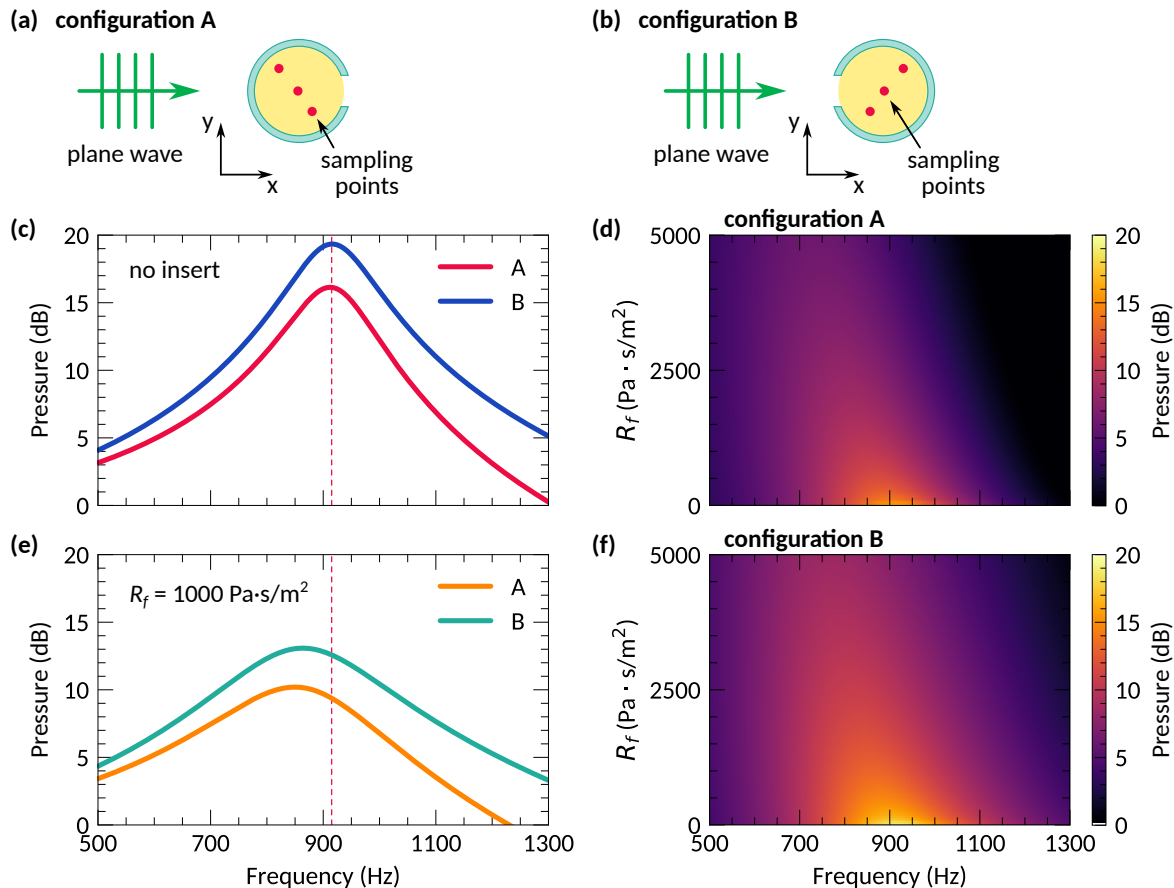

Figure S3. **Standalone resonator.** Schematic geometry of the open system with a standalone resonator oriented (a) "away" from (configuration A) and (b) "towards" (configuration B) the incident field. In both cases the resonators are supplemented by a porous inserts shown by yellow color. Pressure spectra calculated inside the resonators (c) without porous inserts and with inserts characterized by the flow resistivity $R_f = 1000$ Pa·s/m^2. The vertical red lines indicate the pressure peak corresponding to the configuration A without the insert. Pressure spectra calculated inside the resonators as functions of the flow resistivity of the porous inserts for (d) configuration A and (f) configuration B.

When a second resonator is introduced into the system, their coupling results in the splitting of the resonance. As discussed in the main text, one part of the split resonance corresponds to the symmetric mode and shifts towards the lower frequencies with the increase of the coupling strength. The second resonance corresponds to the antisymmetric mode having larger frequency and larger quality factor than the symmetric one. When a porous insert is introduced into one of the resonators within the pair [see Figs. S4(a) and S4(b)], the amplitude of the quasi-BIC in the resonator with the

insert quickly decreases with the increase of the flow resistivity [see Figs. S4(c) and S4(f)]. At the same time, the change of the corresponding amplitude in the resonator without the insert does not change so drastically [see Figs. S4(d) and S4(e)]. In other words, the increase of intrinsic losses in one of the resonators results in the asymmetric excitation of the resonators, as it should be expected.
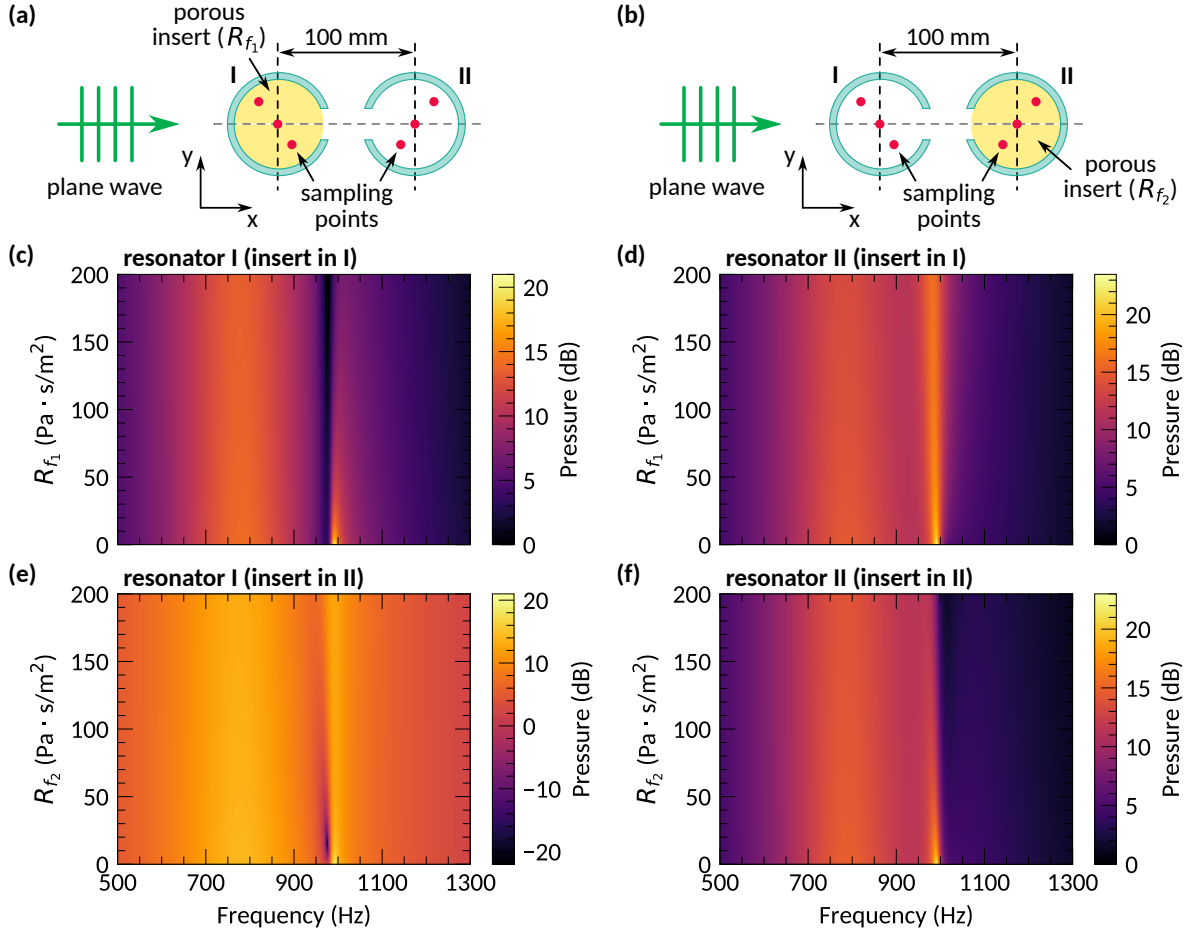

Figure S4. **Tuning of losses in one of the resonators within a pair.** Schematic illustration of the considered open system consisting of two resonators, such that the porous insert is placed inside (a) the resonator I and (b) the resonator II. Pressure spectra for the case when the insert is placed in the resonator I, calculated inside (c) the resonator I and (d) the resonator II. Pressure spectra for the case when the insert is placed in the resonator II, calculated inside (e) the resonator I and (f) the resonator II.

In the case when the inserts are introduced into the both resonators [see Fig. S5(a)], the resonance amplitude also decreases with the increase of the flow resistivity, such that at $R_f = 200$ Pa·s/m^2 the antisymmetric mode becomes indistinguishable. Therefore, tuning of the quasi-BIC via intrinsic losses should be done with materials characterized by the flow resistivity below 10 Pa·s/m^2 or even below 1 Pa·s/m^2. Such values are much smaller than the corresponding values of conventional materials, like rock wool or melamine foam. Hence, the experimental verification should be done

with the inserts occupying only a small part of the resonators' volume, as discussed in the main text.
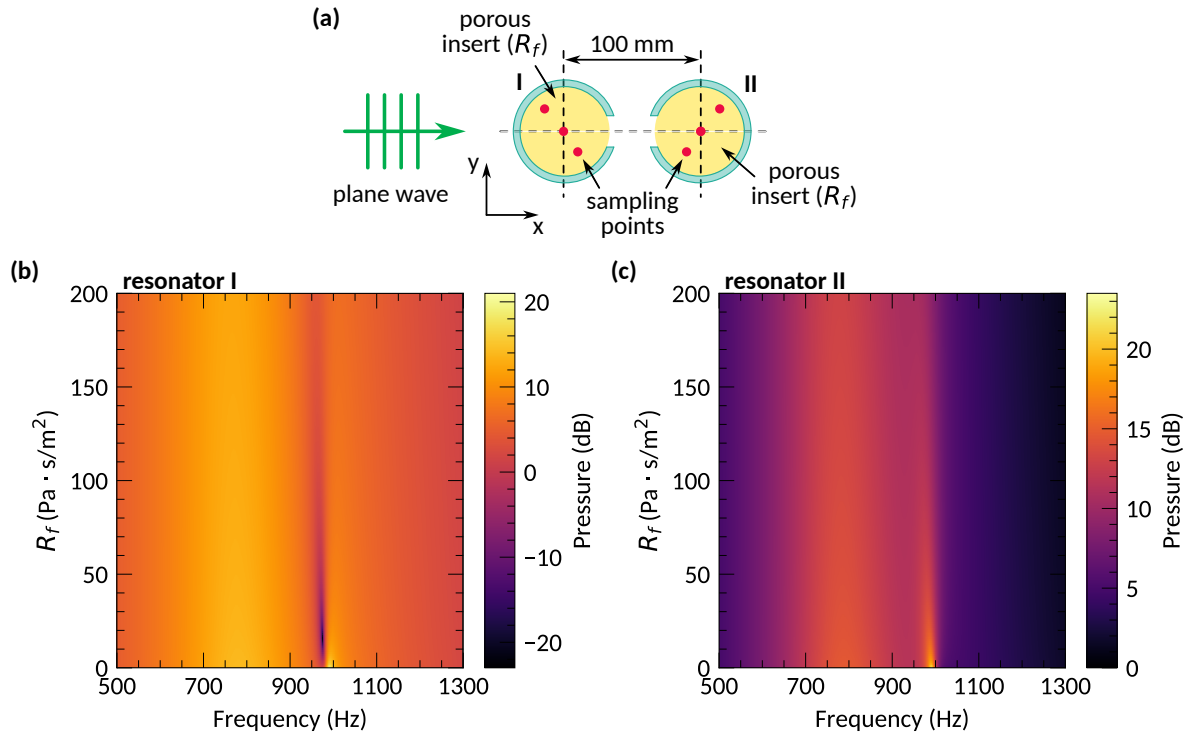

Figure S5. **Tuning of losses in both resonators within a pair.** (a) Schematic illustration of the considered open system consisting of the two resonators supplemented by porous inserts with the flow resistivity R_f. Pressure spectra calculated inside (b) the resonator I and (c) the resonator II.